Materials Today Bio 26 (2024) 101034

Contents lists available at ScienceDirect

Materials Today Bio

journal homepage: www.journals.elsevier.com/materials-today-bio

A multifunctional nanogel encapsulating layered double hydroxide for enhanced osteoarthritis treatment via protection of chondrocytes and ECM

Changxing Liu [a,1], Yawei Sun [d,1], Dengju Li [b], Fan Wang [a], Haojue Wang [a], Senbo An [b,**], Shui Sun [a,b,c,*]

[a] Department of Joint Surgery, Shandong Provincial Hospital, Shandong University, Jinan, Shandong, 250012, China
[b] Department of Joint Surgery, Shandong Provincial Hospital Affiliated to Shandong First Medical University, Jinan, Shandong, 250021, China
[c] Orthopaedic Research Laboratory, Medical Science and Technology Innovation Center, Shandong First Medical University & Shandong Academy of Medical Sciences, Jinan, Shandong, 250117, China
[d] Shandong Key Laboratory of Reproductive Medicine, Department of Obstetrics and Gynecology, Shandong Provincial Hospital Affiliated to Shandong First Medical University, Jinan, Shandong, 250021, China

ARTICLE INFO

Keywords:
Osteoarthritis
Extracellular matrix
Chondrocytes
Layered double hydroxide (LDH)
Strontium (Sr^{2+})
Tannic acid

ABSTRACT

Osteoarthritis (OA) is characterized by progressive and irreversible damage to the articular cartilage and a consecutive inflammatory response. However, the majority of clinical drugs for OA treatment only alleviate symptoms without addressing the fundamental pathology. To mitigate this issue, we developed an inflammation-responsive carrier and encapsulated bioactive material, namely, LDH@TAGel. The LDH@TAGel was designed with anti-inflammatory and antioxidative abilities, aiming to directly address the pathology of cartilage damage. In particular, LDH was confirmed to restore the ECM secretion function of damaged chondrocytes and attenuate the expression of catabolic matrix metalloproteinases (Mmps). While TAGel showed antioxidant properties by scavenging ROS directly. In vitro evaluation revealed that the LDH@TAGel could protect chondrocytes from inflammation-induced oxidative stress and apoptosis via the Nrf2/Keap1 system and Pi3k-Akt pathway. In vivo experiments demonstrated that the LDH@TAGel could alleviated the degeneration and degradation of cartilage induced by anterior cruciate ligament transection (ACLT). The OARSI scores indicating OA severity decreased significantly after three weeks of intervention. Moreover, the IVIS image revealed that LDH@TAGel enhances the controlled release of LDH in a manner that can be customized according to the severity of OA, allowing adaptive, precise treatment. In summary, this novel design effectively alleviates the underlying pathological causes of OA-related cartilage damage and has emerged as a promising biomaterial for adaptive, cause-targeted OA therapies.

1. Introduction

Osteoarthritis (OA) is a chronic disease with high morbidity and clinical burden, affecting approximately 240 million people worldwide, and its prevalence is expected to increase due to the global ageing population [1,2]. The primary clinical manifestations of OA include joint pain, deformity, and dysfunction [3,4]. The deterioration of the extracellular matrix (ECM) of cartilage is considered the hallmark of OA [5]. Under normal physiological circumstances, the articular cartilage has the ability to withstand loads that are multiple times the weight of the body, facilitating a seamless and frictionless articulation of the joint [6]. However, in osteoarthritic conditions, the integrity of the ECM of cartilage is compromised, resulting in a deterioration of its biomechanical characteristics [7]. This phenomenon leads to joint degeneration and the emergence of additional clinical symptoms. At present, there is a lack of efficacious treatments that can reverse the degradation of ECM in OA. In the initial phases of OA, pharmacological intervention is the preferred method [8]. However, its primary objective is to alleviate joint pain in the short term rather than to reverse ECM degradation [9]. In the advanced stages of OA, joint replacement surgery is the sole

* Corresponding author. Department of Joint Surgery, Shandong Provincial Hospital, Shandong University, Jinan, Shandong, 250012, China.
** Corresponding author. Department of Joint Surgery, Shandong Provincial Hospital Affiliated to Shandong First Medical University, Jinan, Shandong, 250021, China.
E-mail addresses: ansenbo@sdfmu.edu.cn (S. An), sunshui@sdfmu.edu.cn (S. Sun).
[1] C. Liu and Y. Sun contributed equally to this work.

https://doi.org/10.1016/j.mtbio.2024.101034
Received 19 November 2023; Received in revised form 20 February 2024; Accepted 19 March 2024
Available online 25 March 2024

viable option [8]. Nonetheless, this approach solely involves the substitution of degenerative cartilage and does not involve its repair, thereby potentially leading to postoperative complications [10]. Consequently, it is imperative to establish a therapeutic regimen that aims to safeguard the ECM from deterioration.

Chondrocytes are the sole cellular component within cartilage [11]. These cells play a crucial role in the remodelling of ECM through both anabolic and catabolic processes [12]. In terms of the anabolic process, chondrocytes actively participate in the synthesis of collagen type 2 (Col2) and aggrecan (Acan), constituents that are essential for endowing cartilage with load-bearing and compressive-resistant properties. Conversely, in the catabolic process, chondrocytes engage in the synthesis of matrix metalloproteinases (Mmps), which contribute to the degradation of the ECM. Overall, a slow turnover of the ECM is observed, characterized by a delicate equilibrium between anabolic and catabolic processes [13]. Nevertheless, the presence of OA disrupts this equilibrium [14]. In addition to causing a deficiency in ECM synthesis, OA also induces an upregulation of Mmps, which degrade the ECM and worsen OA. Strontium (Sr^{2+}) has shown promise in promoting the anabolic process of chondrocytes. Deng et al. developed a scaffold containing Sr^{2+} that effectively promoted the upregulation of ECM markers in chondrocytes [15]. Moreover, strontium ranelate, a drug containing Sr^{2+}, has been proven to significantly alleviate OA symptoms in a randomized controlled clinical trial [16]. Additionally, Sr^{2+} has been reported to alleviate oxidative stress by activating the intrinsic antioxidant system [17]. However, high concentrations of Sr^{2+} can be detrimental because of the induction of cell apoptosis [17]. Therefore, a suitable carrier for the controlled release of Sr^{2+} is needed. Layered double hydroxides (LDHs) are host-guest layered materials formed due to electrostatic attractions between cationic host layers and anionic guest molecules [18]. LDHs show common biocompatibility, good drug load and release properties [19]. Furthermore, LDH materials have shown good potential in treating various diseases, such as nerve repair and osteoporosis [20,21]. In this study, we synthesized LDH using $SrCl_2$ as a divalent cation donor for the drug-free therapy of OA. We hypothesize that Sr^{2+}-containing LDH can maintain a stable concentration of Sr^{2+} within the joints, enhancing the protective effects towards the ECM.

Oxidative stress and cellular apoptosis are commonly observed in conjunction with ECM degradation induced by OA. Inflammatory stimulation leads to an increase in the generation of free radicals, including reactive oxygen species (ROS) and reactive nitrogen species (RNS) [22]. The resultant imbalance between these free radicals and antioxidant systems is defined as oxidative stress [23]. Prior research has investigated the relationship between oxidative stress and ECM degradation [24]. The high reactive properties of ROS not only directly causes ECM damage but also leads to telomere instability and replicative senescence in chondrocytes, indirectly impairing their ECM synthesis function [25]. Additionally, research has demonstrated that oxidative stress has the potential to induce cellular apoptosis through both mitochondria-dependent and mitochondria-independent pathways [26]. The apoptotic process consequently diminishes the number of functional chondrocytes and exacerbates the deterioration of cartilage. Numerous studies have been conducted to explore the potential of targeting oxidative stress and apoptosis as therapeutic approaches for OA, yielding promising results [24,27,28]. These results suggest that we should develop bioactive materials against OA by focusing on reducing oxidative stress and inhibiting apoptosis. However, due to the diverse sources of ROS production, the efficacy of single intervention can be limited. Apart from the Sr^{2+} mentioned above, we introduced tannic acid (TA). It is a natural antioxidant demonstrated to directly neutralize ROS [29]. Notably, studies have shown that TA can interact with proteins, limiting the enzyme activity of Mmps and thereby reducing their negative effects on the ECM [30]. In synergy with Sr^{2+} and TA, the composite material might offer enhanced protection to the ECM, potentially alleviating oxidative stress-induced damage.

Intra-articular injections are highly valued for their high bioavailability and low systemic adverse effects. Nevertheless, there remains a notable obstacle: the rapid elimination of small molecules from joints through vascular and lymphatic routes [31,32]. To address this, many studies have focused on designing composite biomaterials with improved sustained-release characteristics. For example, Li et al. constructed hydrogels using gelatin and gallic acid to endow them with sustained liposome release capabilities, greatly extending the effective treatment duration [33]. Additionally, the incorporation of responsive elements into the carrier could further achieve drug delivery with intelligence and precision. It has been reported that a pH-responsive gel based on a carboxymethyl hexanoyl chitosan/hyaluronic acid polymer could release inner berberine faster when the pH of synovial fluid decreases, allowing treatment of advanced OA [34]. Moreover, many other materials have been engineered with responsive release capabilities that have shown positive outcomes. These materials can respond to various triggers, such as temperature, enzymes, light, and magnetism [35–37]. Gelatin, a degradable natural protein, contains RGD sequences that promote cell adhesion and growth, has excellent biocompatibility and has been extensively used in tissue engineering [38]. Recent studies indicate that gelatin can degrade more rapidly in the presence of high Mmps levels, thus accelerating the release of encapsulated drugs [39]. Given that Mmps levels are notably elevated in OA-affected joints, gelatin-based carriers might present promising prospects for inflammation-responsive drug release.

In this study, we crosslinked gelatin with TA to form TAGel, aiming to enhance the stability and functionality of the carrier. By encapsulating LDH within TAGel, we crafted LDH@TAGel, a material designed for the intelligent release of TA and LDH in accordance with OA severity. Specifically, the crosslinking of gelatin with TA, coupled with the inherent properties of LDH, enhances the sustained-release characteristics of LDH@TAGel. Simultaneously, the gelatin carrier is engineered to degrade faster in the presence of elevated Mmps levels in osteoarthritic joints, giving LDH@TAGel an inflammation-responsive release feature. Using IL-1β-stimulated chondrocytes as in vitro model, we investigated the effects of LDH@TAGel on the ECM secretion, oxidative stress, and cell apoptosis of the chondrocytes. Furthermore, by employing the anterior cruciate ligament transection (ACLT) mice as in vivo OA model, we introduced LDH@TAGel into the joint cavity and assessed its therapeutic effectiveness based on cartilage integrity. We hypothesize that LDH@TAGel holds the potential to alleviate the inflammatory microenvironment, safeguard ECM and chondrocytes, and offer promising prospects in drug-free, smart-release therapy of OA.

2. Experimental section

2.1. General materials

$SrCl_2$ and $AlCl_3$ were purchased from Tianjin Kemiou Co. Ltd. Tannic acid was purchased from Sigma-Aldrich. Gelatin was purchased from Shanghai Aladdin reagent Co. Ltd. 2,2-diphenyl-1-picrylhydrazyl (DPPH) free radical was purchased from Solarbio for the DPPH assay. Reagents for cell culture were obtained from Gibco (USA), including Dulbecco's Modified Eagle Medium/Nutrient Mixture F-12 (DMEM/F12, C11330500BT, Gibco), foetal bovine serum (FBS, 10099-141C, Gibco), and penicillin/streptomycin (P/S, 15140122, Gibco).

2.2. Synthesis of LDH and LDH@TAGel

For the synthesis of LDH, solutions of $SrCl_2$ (0.6 M) and $AlCl_3$ (0.2 M) were mixed at a ratio of 1:1, and NaOH solution (0.15 M) was added drop by drop under strong mechanical stirring. Then, the mixture was heated at 100 °C for 16 h. The resultant LDH was purified using suction filtration to remove unreacted ions and large particles. For synthesis of LDH@TAGel, 90 mg of gelatin was ultrasonically dispersed in 900 μL of phosphate-buffered saline (PBS) at 60 °C. Next, 100 μL of LDH was added and stirred until a homogeneous solution was achieved.

Separately, 5 mg of tannic acid was dissolved in 1000 μL of deionized water at 60 °C. Finally, equal volumes of the two prepared solutions were rapidly mixed and cooled to room temperature to form LDH@TAGel.

2.3. Characterization of LDH and LDH@TAGel

Elemental concentrations of Sr^{2+} and Al^{3+} in LDH solution were determined using inductively coupled plasma–optical emission spectrometry (ICP–OES; iCAP 7400, Thermo Fisher, USA). The X-ray diffraction (XRD) patterns were obtained on an X-ray diffractometer (SmartLab, Rigaku, Japan) adopting Cu Kα radiation with a wavelength of 0.1541 nm. XRD was performed in the scanning range of 5–80° at a scanning rate of 5.0° min^{-1} and a step size of 0. 02°. The morphological structure of LDH was assessed via transmission electron microscopy (TEM, 200 kV, JEM-F200, JEOL, Japan). The structure of LDH@TAGel was analysed using scanning electron microscopy (SEM, HITACHI Regulus 8100, Japan). All samples were prepared after freeze-drying and performed with gold sputter-coating. Hydrodynamic diameter was measured using dynamic light scattering (DLS, Zetasizer Nano ZS90, Malvern, UK). Fourier transform infrared spectroscopy (FTIR, Vertex 70 FTIR spectrophotometer, Bruker, Germany) was employed to investigate the chemical structure of various materials. The assessment of the viscosity was performed using a rheometer (Haake Mars60, Thermo Fisher, Germany) at a shear rate of 0.01–100/s at 37 °C. For the release experiment, 3 ml of LDH stock solution was dialyzed in 300 ml of PBS, with PBS being replaced at each time point, and the concentration of Sr^{2+} was determined by ICP-OES. The cumulative release amount at each time point was calculated to determine the release pattern of Sr^{2+} from LDH. 100 mg of TAGel was immersed in 10 ml of PBS, and the absorbance at 300 nm of the supernatant was measured at different time points to calculate the release curve of TA from TAGel.

2.4. Isolation and culture of primary chondrocytes

Primary chondrocytes were procured from mice aged 4–10 days. The cartilage from the knee joint and rib was isolated on a sterile operating table and subsequently fragmented into small pieces. Following a thorough wash with PBS, the fragments were subjected to sequential digestion with 0.25% trypsin (D03-X040, BasalMedia) for 30 min and 0.2% type II collagenase (C8150, Solarbio) for 6 h under incubation at 37 °C, as previously described. Following centrifugation to remove the supernatant, the cartilage cells were cultured in DMEM/F12 medium with 10% foetal bovine serum and 1% penicillin–streptomycin at 37 °C and 5% CO_2 in a cell culture incubator, with the medium being refreshed every 2 days. Passaging was conducted upon reaching 80%–90% cell confluence. Third-passage chondrocytes were identified through Alcian blue staining (G1560-3, Solarbio) and immunofluorescence and utilized for subsequent experiments.

2.5. Cell viability assay

A Cell Counting Kit-8 (CCK-8, E-CK-A362, Elabscience) assay was employed to assess the cytotoxicity of our materials. Chondrocytes were cultured in a 96-well plate at a density of 5000 cells per well and incubated for 12 h. Subsequently, the original culture medium was replaced with complete culture medium mixed with LDH or LDH@TAGel at varying concentrations (0, 5, 10, 25, 50, 100, 200 mg/ml). The cells were then incubated with the culture medium above for 1, 3, and 5 days. Following the manufacturer's instructions, the cells were treated with a 10% CCK-8 solution for 2 h, and the absorbance at 450 nm was measured using a microplate reader (TECAN SPARK). The proportion of living and dead cells on Day 5 was determined using a Calcein-AM/PI double staining kit (HR0444, Biolab Technology Co., Ltd., Beijing) according to the manufacturers' instructions.

2.6. Western blot

Cells were exposed to IL-1β (10 ng/ml, 211-11B, Peprotech) and various material components for 72 h. The cells were lysed using ice-cold RIPA lysis buffer (R0020, Solarbio) with 1% protease inhibitor (CW2200; Cwbio) and 1% phosphatase inhibitor (CW2383; Cwbio) for a period of 30 min. The resultant pure protein solution was obtained through centrifugation at 12,000 rpm for 15 min, and the concentration was determined using a BCA assay kit (PC0020, Solarbio). The proteins were subjected to electrophoresis on a 7.5% SDS–PAGE gel, transferred onto a polyvinylidene fluoride (PVDF) membrane, and blocked with 5% skim milk for 1 h. The membrane was incubated with primary antibodies against detected proteins overnight at 4 °C. Primary antibodies included Col2 (28459-1-AP, Proteintech), Sox9 (ab185966, Abcam), Mmp13 (18165-1-AP, Proteintech), Nrf2 (16396-1-AP, Proteintech), Keap1 (10503-2-AP, Proteintech), Pi3k (4257S, CST), P-Pi3k (17366S, CST), Akt (10176-2-AP, Proteintech) and P-Akt (4060S, CST). Followed by a subsequent incubation with Anti-Rabbit IgG (SA00001-2, Proteintech) or Anti-Mouse IgG (SA00001-1, Proteintech) at room temperature for 1 h, the blot bands were visualized by chemiluminescent HRP substrate (WBKLS0500, Merck Millipore) using a ChemiDoc™ touch imaging system (Bio-Rad, Hercules, CA, USA). The intensity of the bands presented on the immunoblot was analysed using ImageJ software (version 1.51).

2.7. Alcian blue staining

The culture conditions of the cells remained the same as above, while the stimulation duration was prolonged to two weeks, with the culture medium with IL-1β and distinct material components being refreshed every three days. The cells were subsequently fixed with 4% paraformaldehyde (P1110, Solarbio) for 15 min and stained with the Alcian blue staining kit (G1560-3, Solarbio) following the manufacturer's guidelines. Subsequently, the cells were washed with PBS and imaged using an optical microscope (NIB620-FL, Nexcope).

2.8. Immunofluorescence

The cells were seeded onto preplaced coverslips in a 12-well plate and subjected to the same treatment as previously described. Subsequently, the chondrocytes were fixed with 4% paraformaldehyde for 15 min, permeabilized with 0.5% Triton X-100 (T8200, Solarbio) for 20 min, and blocked with 3% bovine serum albumin at room temperature for 1 h. The primary antibody, including Col2 (28459-1-AP, Proteintech) and Mmp13 (18165-1-AP, Proteintech), was diluted to a concentration of 1:200 and used to incubate cells overnight at 4 °C, followed by incubation with a fluorescently labelled secondary antibody (ZF-0511; 1:500; OriGene Technologies, Inc.) at room temperature while being protected from light. After the samples were mounted with DAPI-containing medium (KGF0281, KeyGEN, China), fluorescence images were captured using a fluorescence microscope (NIB620-FL, Nexcope).

2.9. DPPH assay

The assessment of the free radical scavenging capacity of the materials was conducted through the 1,1-diphenyl-2-picrylhydrazyl (DPPH) assay. A 100 μmol/L DPPH/ethanol solution was first prepared. Subsequently, 200 μL of the DPPH solution and 20 μL of various material components at different concentrations were added to individual wells of a 96-well plate. Following a 30-min incubation at room temperature, the absorbance at 517 nm was measured using a microplate reader (TECAN SPARK).

2.10. ROS and RNS detection

Intracellular reactive oxygen species (ROS) were detected by the

DCFH-DA probe (s0033, Beyotime). Following a 24-h stimulation of cells with IL-1β (10 ng/ml) and various material components, cells were loaded with DCFH-DA probe (10 μM) in serum-free DMEM/F12 and incubated at 37 °C for 20 min. Subsequently, the cells were costained with Hoechst (C1028, Beyotime) for 10 min to label the nuclei. After the cells were washed, IL-1β was reapplied for 10 min, and the cells were observed under a fluorescence microscope (NIB620-FL, Nexcope). The Griess assay employed a nitric oxide detection kit (YT286, Biolab Technology Co., Ltd., Beijing) to quantify the concentration of reactive nitrogen in the supernatant of the cell culture. The procedure involved the addition of 50 μL of Reagent I, 50 μL of Reagent II, and 50 μL of the cell culture supernatant to individual wells of a 96-well plate, followed by measurement of the absorbance at 540 nm.

2.11. Flow cytometry to detect apoptosis

The cell treatment protocol was executed in a manner consistent with the above procedures. Cell apoptotic rate was analysed using an Annexin V-FITC/PI apoptosis detection kit (KGA106, KeyGEN). Specifically, after a 24-h stimulation duration, cells were harvested through digestion with 0.25% trypsin devoid of EDTA, inclusive of nonadherent cells. After centrifugation, cells from each group were resuspended in 500 μL of binding buffer, followed by the addition of 5 μL of Annexin V-FITC and 5 μL of propidium iodide. The mixture was gently agitated and incubated at room temperature for 10 min in the absence of light. Subsequently, flow cytometry was performed using Cytek Aurora (Cytek Biosciences), and apoptotic rate was analysed using FlowJo software.

2.12. RNA-seq analysis of chondrocytes

The extraction of total RNA was performed using RNAiso Plus reagent (Catalog No. 9109, Takara Bio Inc.) following the manufacturer's protocol. The purity and quantification of RNA were assessed using a NanoDrop 2000 spectrophotometer (Thermo Scientific, USA), while the integrity of RNA was evaluated using an Agilent 2100 Bioanalyzer (Agilent Technologies, Santa Clara, CA, USA). Subsequently, libraries were constructed using the VAHTS Universal V6 RNA-seq Library Prep Kit according to the manufacturer's instructions. Transcriptome sequencing and analysis were conducted by OE Biotech Co. Ltd. (Shanghai, China). Differential expression analysis was conducted utilizing the DESeq2 package. A threshold of Q value < 0.05 and fold change >2 or fold change <0.5 was established to identify significantly differentially expressed genes (DEGs). To illustrate the expression patterns of genes across various groups and samples, we performed hierarchical cluster analysis of the DEGs using R (v 3.2.0). With the hypergeometric distribution, KEGG pathway enrichment analysis of differentially expressed genes (DEGs) was conducted through the implementation of R (v 3.2.0). Additionally, gene set enrichment analysis (GSEA) was performed using GSEA software. This analysis employed a pre-established gene set, whereby the genes were ranked based on the extent of differential expression observed in the two distinct sample types. Subsequently, an assessment was conducted to determine if the predefined gene set exhibited enrichment at either the uppermost or lowermost positions within the ranking list.

2.13. RT-qPCR

Quantitative Reverse Transcription Polymerase Chain Reaction (RT-qPCR) technique was applied to measure mRNA levels in chondrocytes. Total RNA was extracted using the RNAiso Plus reagent (9109, Takara) following the guidelines provided by the manufacturer. Subsequent cDNA synthesis was achieved through the reverse transcription process utilizing the PrimeScript™ RT Reagent Kit (RR047A, Takara). RT-qPCR was performed by SYBR Green Premix Pro Taq HS qPCR Kit (11701, AG) with a LightCycler 480II (Roche) to determine mRNA expression. GAPDH served as the internal reference gene. The relative quantification of mRNA expression was performed employing the 2-ΔΔCt calculation method. All primer sequences used for this study are available by request.

2.14. IVIS imaging

Cy5 (R–CY2009, RuixiBiotech, China) was affixed to LDH through magnetic stirring at a temperature of 50 °C for 12 h. The labelled LDH was employed in the synthesis of LDH@TAGel. LDH and LDH@TAGel were administered to the knee joints of mice via intra-articular injection. The injected materials contained equivalent quantities of LDH to ensure uniform basal fluorescence intensity. Following appropriate time intervals (0 h, 6 h, 12 h, 24 h, 48 h, 72 h), the residual fluorescence intensity was measured using an IVIS system (BLT Aniview 100, Biolight Biotechnology, China). The region of interest (ROI) was delineated within the knee area. The radiant efficiency was computed as [p/s/cm2/sr]/[μW/cm2] and normalized by the fluorescence intensity at 0 h.

2.15. Osteoarthritis animal model

All experiments on mice were conducted following the protocol approved by the ethics committee of Shandong Provincial Hospital Affiliated to Shandong First Medical University (No. 2022-094, Shandong, China). 20 male C57/BL6 mice, aged 8–9 weeks, were used to establish an osteoarthritis model via the anterior cruciate ligament transection (ACLT) method on the right knee. The control group underwent exposure of the anterior cruciate ligament followed by suturing. The mice were randomly allocated to five groups: the control group, ACLT group, ACLT + TAGel treatment group, ACLT + LDH treatment group, and ACLT + LDH@TAGel treatment group. The treatment groups were subjected to intra-articular injection of 15 μL of various materials into the joint cavity two weeks post-surgery, with a 4-day interval between injections, totalling 5 injections. The control group and OA group received an equivalent volume of saline injection. Following the final injection, the mice were euthanized, and the right knee joint was harvested for subsequent experiments after systemic polyformaldehyde perfusion.

2.16. Histological assessment

The knee joint tissues were subjected to a 48-h immersion in 4% paraformaldehyde, followed by a 3-week immersion in a decalcification solution containing 10% EDTA. The decalcified samples were then embedded in paraffin and sectioned into 4 μm thick sections. For histological examination, the samples were stained using the H/E and Safranin O/Fast Green staining methods. The Osteoarthritis Research Society International (OARSI) scoring system was employed to quantitatively assess the severity of osteoarthritis. The TUNEL assay and immunohistochemical (IHC) staining were conducted to detect DNA fragmentation and protein expression, respectively. For TUNEL, samples of knee joints underwent permeabilization, endogenous peroxidase inactivation, and labeling of DNA ends in apoptotic cells, with signals visualized via DAB staining. The IHC procedure involved deparaffinization, rehydration, antigen retrieval and peroxidase inactivation in tissue sections, followed by incubation with primary antibodies (anti-Col2, anti-Mmp13) and a secondary antibody. DAB staining was employed for signal detection, which was then observed under a microscope.

2.17. Statistical analysis

Quantitative data are presented as the mean ± standard deviation (SD). The analysis of variance (ANOVA) was employed for comparisons among multiple groups. A p value of less than 0.05 was deemed statistically significant. The statistical analyses were conducted using GraphPad Prism 8.0 software.

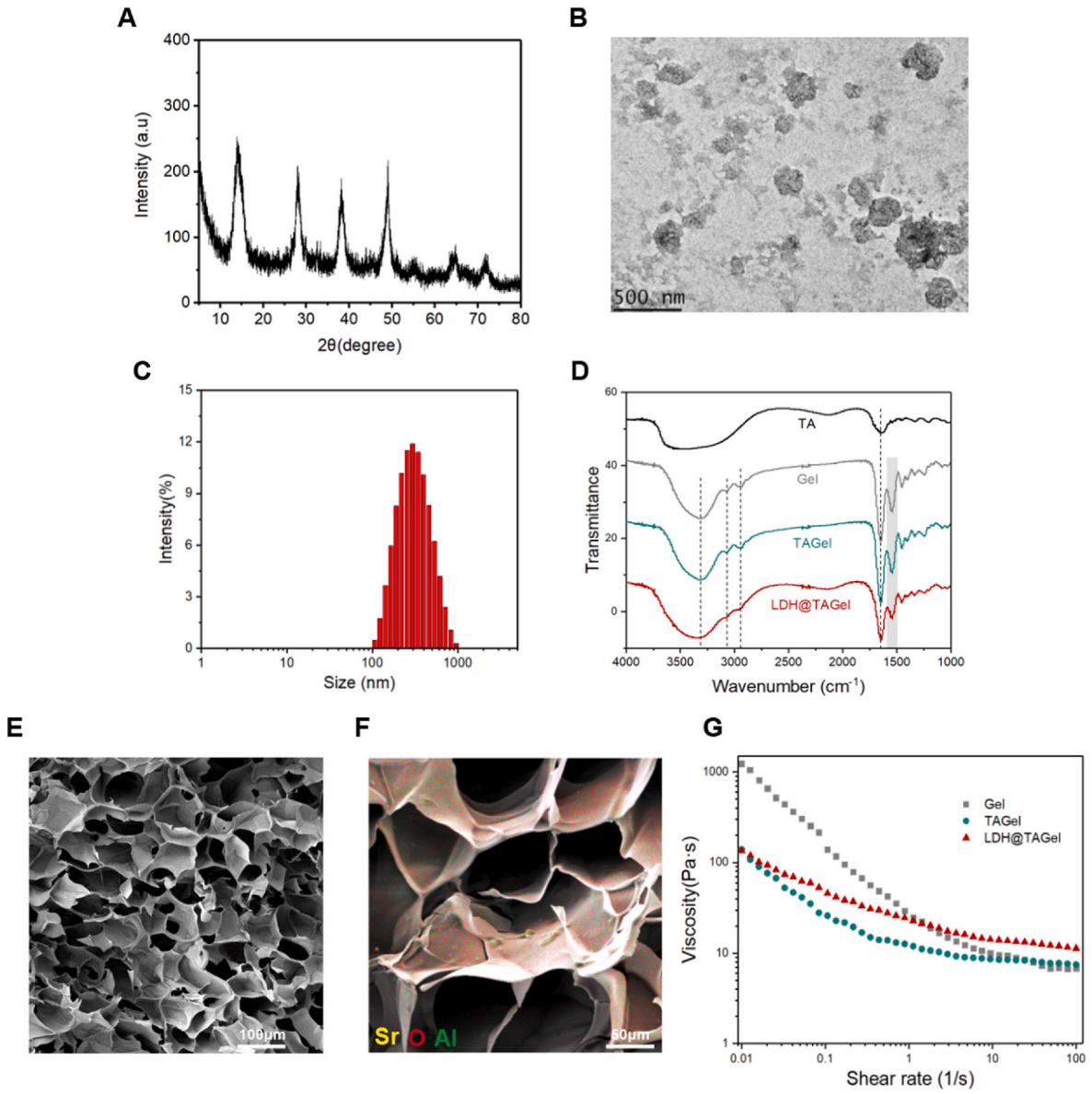

Fig. 1. Characterization of LDH and LDH@TAGel nanogels. (A) XRD pattern of LDH. (B) TEM image of LDH. (C) Size distribution of LDH. (D) FTIR spectra of TA, Gel, TAGel and LDH@TAGel. (E) SEM and (F) elemental mapping images of LDH@TAGel. (G) Viscosity changes of all samples.

3. Results and discussion

3.1. Characterization of LDH and LDH@TAGel nanogels

The LDH was synthesized by a hydrothermal method. The element concentrations were determined by ICP–OES. The contents of Sr and Al in LDH were 14.15 ± 0.0363 mM and 2.033 ± 0.0362 mM, respectively. The structure of LDH was investigated with XRD. The XRD results demonstrated that LDH possesses a good lattice structure (Fig. 1A), and diffraction reflections (003), (006), (110) and (203) of the LDH structure can be observed in the XRD patterns. The morphology of Sr-LDH was investigated with TEM. The TEM image in Fig. 1B shows that the LDH was successfully constructed with a hexagonal sheet structure. The hydrodynamic diameter of LDH is approximately 300 nm, as shown in Fig. 1C. The LDH encapsulated with TAGel (LDH@TAGel) was obtained to avoid premature clearance in the joint cavity. The chemical structure of TAGel was investigated with FTIR, as shown in Fig. 1D. There are abundant amino groups in gelatin. The N–H stretching was located at 3333 cm^{-1}, and the peak from 1592 cm^{-1} to 1488 cm^{-1} was assigned to N–H bending (amide II). The peaks of $–CH_2-$ for gelatin appeared at 3068 cm^{-1} and 2939 cm^{-1}. The peaks at 1646 cm^{-1} were attributed to the aromatic C═C from both gelatin and TA [40]. The morphology of the freeze-dried LDH-loaded TAGel (LDH@TAGel) was observed by SEM. The distribution of LDH on the TAGel was observed by elemental mapping. The TAGel showed a pore structure with a pore size of approximately 75 μm (Fig. 1E), and the LDH was homogeneously distributed in the TAGel (Fig. 1F). Gelatin was used as the based material at a concentration of 100 mg/ml to synthesize LDH@TAGel. As shown in Fig. 1G, the viscosities of all solutions were reduced when the shear rate increased, suggesting a shear-thinning property due to the destruction of the gel network. Notably, the shear-thinning property of the gel weakens when TA is added and further weakens after LDH is added. The results showed that the addition of TA and LDH increased the stability of the gel network. Furthermore, it's been reported that knee synovial fluid exhibits high zero shear viscosity (6–60 Pa·s) and demonstrates shear thinning with increasing shear rates [41]. The viscosity of LDH@TAGel with a concentration of gelatin at 100 mg/ml is from 10 to 100 Pa·s at shear rate of 0.01–100 s^{-1}, displaying shear-thinning behavior. This

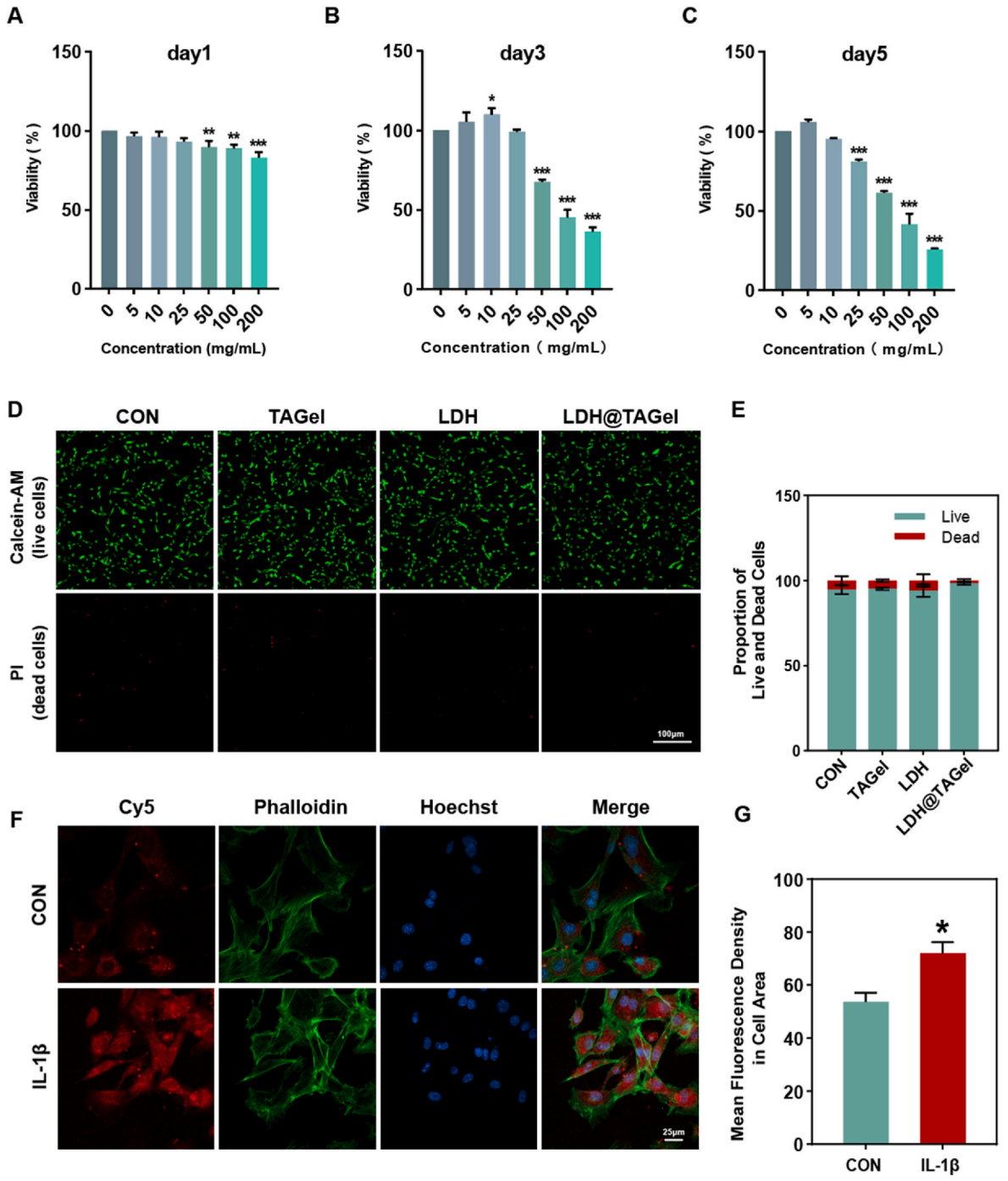

Fig. 2. In vitro biocompatibility and cellular uptake behavior of LDH@TAGel. CCK-8 assay of chondrocytes incubated with LDH@TAGel on Day 1 (A), Day 3 (B), and Day 5 (C). Data were presented as mean ± SD (n = 3). *, $p < 0.05$, **, $p < 0.01$, and ***, $p < 0.001$, compared with the 0 mg/mL LDH@TAGel group (D) Fluorescence images of chondrocytes stained with Calcein-AM (green, live cells) and PI (red, dead cells) after incubation with various materials for 5 days. (E) Quantification of the living/dead cell proportion with Calcein-AM/PI staining. Data were presented as mean ± SD (n = 3). (F) Confocal microscopy images showing the colocalization of LDH@TAGel (Cy5, red), the cytoskeleton (Phalloidin, green) and the nucleus (Hoechst, blue). (G) Quantification of the mean fluorescence density within the cell area. Data were presented as mean ± SD (n = 3) *, $p < 0.05$, compared with the control group. (For interpretation of the references to color in this figure legend, the reader is referred to the Web version of this article.)

suggests that LDH@TAGel with optimized concentration and ratio of raw material closely mimics the rheological properties of synovial fluid, demonstrating great potential in intra-articular applications. Finally, the release profiles of Sr^{2+} from LDH and TA from gelatin were examined in vitro. Sr^{2+} exhibited an immediate and rapid release within the first 6 h, achieving over 80% release ratio, and plateauing thereafter, indicating a burst release mechanism (Fig. S1A). In contrast, TA release from TAGel was gradual, starting with a slower increase within the first 12 h, followed by a steady ascent, and then tapering off, suggesting a slower, continuous release mechanism (Fig. S1B). This S-shaped curve of TA release kinetics is attributable to the progressive degradation of TAGel. Further, the integration of LDH into TAGel may enhance the sustained release capability of Sr^{2+}, moderating the initial burst to ensure a prolonged therapeutic effect.

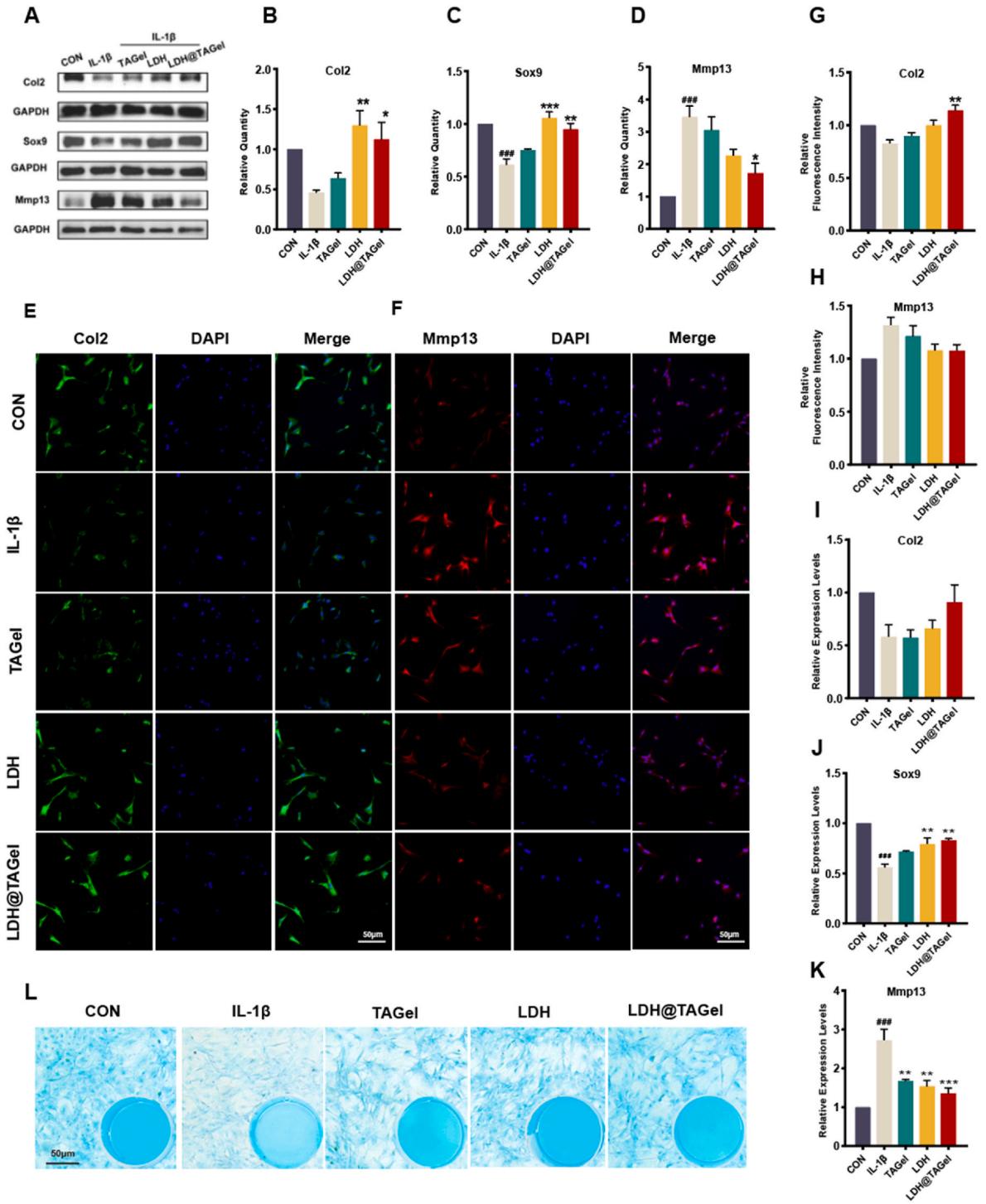

Fig. 3. The ECM-protective effects of LDH@TAGel on chondrocytes. (A) The protein levels of chondrocyte anabolic markers (Col2 and Sox9) and a matrix degeneration marker (Mmp13). (B–D) Quantitative western blot results normalized to GAPDH and data were presented as mean ± SD (n = 3). *, $p < 0.05$, **, $p < 0.01$, and ***, $p < 0.001$, compared with the IL-1β group; ###, $p < 0.001$, compared with the control group (E, F) Cell immunofluorescence images of chondrocytes stained with Col2 (E, green) and Mmp13 (F, pseudocoloured red) antibodies. Nuclei were counterstained with DAPI (blue). (G, H) Quantification of immunofluorescence images. Data were presented as mean ± SD (n = 3). **, $p < 0.01$, compared with the IL-1β group. (I, J and K) RT-qPCR analysis showing mRNA levels of Col2 (I), Sox9 (J), and Mmp13 (K) in different groups. Quantitative results were normalized to GAPDH and data were presented as mean ± SD (n = 3). *, $p < 0.05$, **, $p < 0.01$, ***, $p < 0.001$ compared with the IL-1β group; ###, $p < 0.001$, compared with the control group. (L) The Alcian blue staining results depicted through macroscopic images (right lower pictures) and light microscopy images (large pictures). (For interpretation of the references to color in this figure legend, the reader is referred to the Web version of this article.)

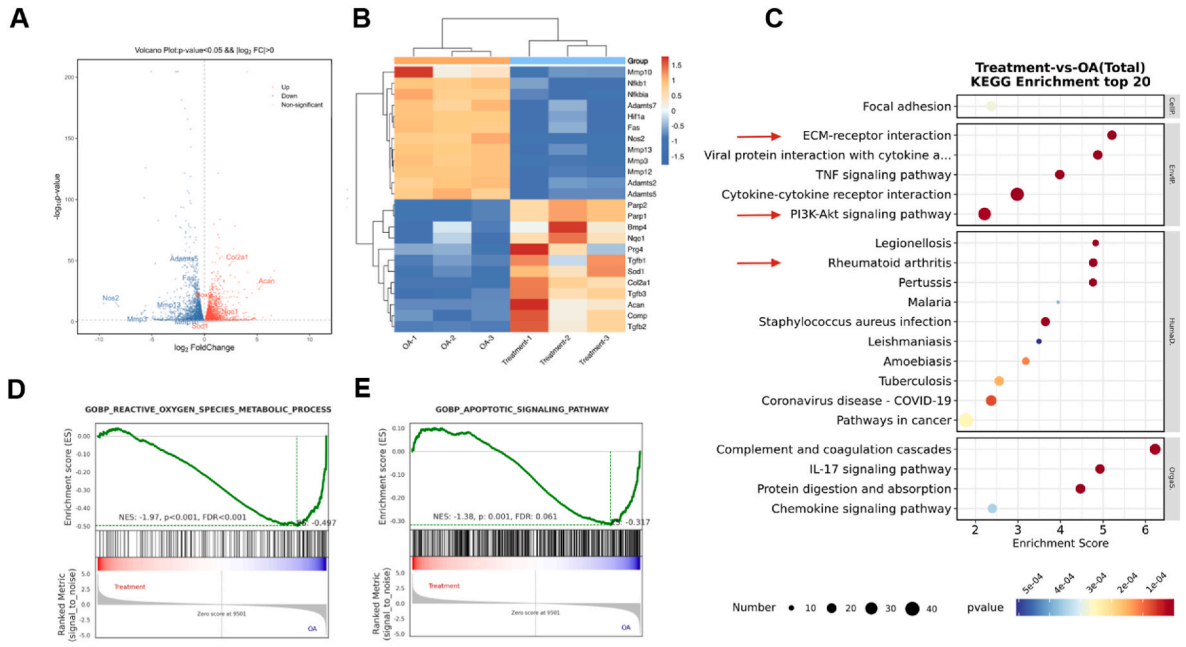

Fig. 4. Transcriptional analysis of chondrocytes by RNA-seq. (A) Volcano plots of differentially expressed genes in IL-1β- and LDH@TAGel-treated chondrocytes (treatment group) compared with IL-1β-treated chondrocytes (OA group). The threshold was set as a p value ≤ 0.05 and $|\log_2\text{-fold change}| \geq 1$. (B) Heatmap of differentially expressed genes of the OA group and treatment group. (C) KEGG pathway enrichment analysis of the OA group and treatment group. (D, E) Gene set enrichment analysis of oxidative stress- and apoptosis-related genes.

3.2. Cytocompatibility in vitro

The cytocompatibility of LDH@TAGel towards chondrocytes was first evaluated. Cells were incubated in culture medium containing LDH@TAGel at a series of concentrations (0, 5, 10, 25, 50, 100 and 200 mg/mL). A CCK-8 assay was used to quantify cell viability after 1, 3, and 5 days (Fig. 2A, B, C). The viability reached 110% ± 4.07 at a concentration of 10 mg/mL on Day 3 (Fig. 2B), implying satisfactory cytocompatibility at this concentration. Nevertheless, a decrease in cell viability was observed when the concentration was higher than 25 mg/mL (80.96% ± 1.33%, Day 5) (Fig. 2C). Based on these data, the safe and cell-affinitive concentration of LDH@TAGel should be less than 25 mg/mL. The LDH alone also exhibited good cytocompatibility, as shown in Fig. S2. We further employed the live/dead cell staining assay to confirm the viability of chondrocytes at the concentration of 10 mg/mL. The proportion of living chondrocytes treated with TAGel and LDH were 95.20% ± 0.68% and 94.07% ± 3.71%, respectively, and did not exhibit significant changes compared with that of the control group (94.61% ± 2.50%) (Fig. 2D and E). A higher proportion of living cells was observed in the LDH@TAGel-treated cells (98.40% ± 0.87%), indicating the excellent cytocompatibility of LDH@TAGel. In summary, our findings demonstrate that LDH@TAGel exhibits favourable cytocompatibility at a concentration of 10 mg/mL. LDH@TAGel with the concentration of 10 mg/mL was chosen for subsequent experiments.

3.3. Cellular uptake behavior

Furthermore, the LDH was labelled with Cy5 for fluorescence localization to track its cellular uptake activity. The nuclei and actin cytoskeleton of the cells were co-stained with Hoechst and Phalloidin. The chondrocytes were treated with or without the inflammatory cytokine IL-1β. Then, LDH(Cy5)@TAGel was added to these chondrocyte models. The cytoplasmic localization of the LDH(Cy5)@TAGel serves as evidence for their affinity towards chondrocytes (Fig. 2F). Remarkably, LDH@TAGel showed a more advantageous distribution within IL-1β-stimulated chondrocytes. The intensity of the red fluorescence was markedly higher in chondrocytes treated with IL-1β compared to those without IL-1β treatment (control group) with a statistically significant difference (Fig. 2G). This suggests an enhanced affinity of Cy5-modified LDH to inflammatory cells, which should be attributed to accelerating degradation of TAGel in response to Mmps in the inflammatory environment, resulting in more LDH being released. LDH with nanoscale dimensions possesses the ELVIS (**e**xtravasation through **l**eaky **v**asculature and subsequent **i**nflammatory cell-mediated **s**equestration) effect, thereby enhancing its uptake by the cells.

3.4. Protective effect on IL-1β-induced ECM degradation

ECM, as the key component in providing joint weight-bearing capacity, is in a dynamic homeostasis between synthesis and breakdown [42]. Chondrocytes play an important role in this intricate process by both producing and breaking down the ECM. In the context of OA, upregulated inflammatory factors (IL-1β) were proven to upset this balance [43]. Specifically, the diminished expression of the transcription factor Sox9 leads to reduced secretion of collagen II (Col2) and aggrecan (Acan), which are the primary constituents of the ECM [44,45]. Additionally, there is an elevation in Mmp13, an enzyme responsible for ECM degradation, ultimately resulting in cartilage degeneration and a compromised load-bearing ability [46]. In this study, chondrocytes were subjected to IL-1β treatment at a concentration of 10 ng/ml to mimic inflammatory conditions in vitro [47]. Then, various materials were introduced and incubated for 72 h. The protein expression levels of Sox9, Col2 and Mmp13 were assessed by western blot and immunofluorescence techniques. Sox9 and Col2 expression was significantly decreased upon stimulation with IL-1β. In the groups treated with LDH and LDH@TAGel, these two markers were upregulated (Fig. 3A, B, C). However, no significant upregulation was observed in the TAGel-treated group. These findings provide evidence that LDH@TAGel effectively restores the ECM secretory function of chondrocytes under IL-1β stimulation, primarily through the action of LDH. Additionally, intervention with IL-1β resulted in an increase in the expression of the Mmp13, while TAGel, LDH and LDH@TAGel reduced it to a progressively greater extent (Fig. 3A and D), further confirming their protective function by impeding the synthesis of catabolic enzymes. The levels of

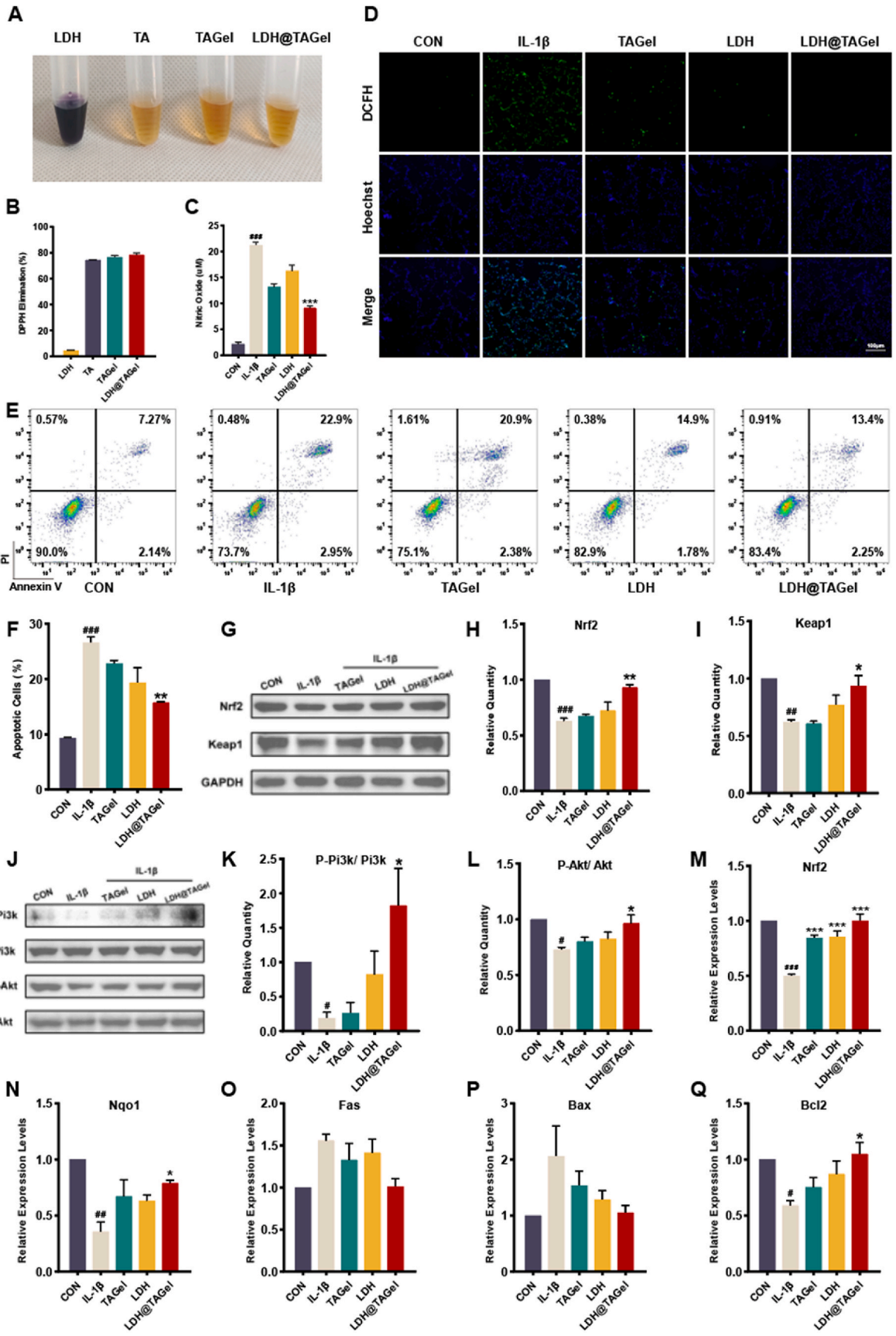

(caption on next page)

Fig. 5. Antioxidative and antiapoptotic functions of LDH@TAGel. (A) DPPH solution supplemented with LDH, TA, TAGel and LDH@TAGel. (B) DPPH elimination rates of LDH, TA, TAGel and LDH@TAGel. Data were presented as mean ± SD (n = 3). (C) RNS content in the supernatants of culture medium measured by Griess assays. Data were presented as mean ± SD (n = 3). ***, $p < 0.001$, compared with the IL-1β group; ###, $p < 0.001$, compared with the control group (D) Fluorescence images of ROS levels in chondrocytes incubated with or without IL-1β and various materials, with detection by a DCFH-DA probe (green) and costaining with nuclei (Hoechst, blue). (E, F) Flow cytometry results (E) of chondrocytes stained with Annexin V-FITC/PI. The apoptosis rate (F) was defined as late apoptosis plus early apoptosis. FITC−/PI+: dead cells, FITC+/PI+: late apoptosis, FITC−/PI−: viable cells, FITC+/PI−: early apoptosis. Data were presented as mean ± SD (n = 3). **, $p < 0.01$, compared with the IL-1β group; ###, $p < 0.001$, compared with the control group (G–I) Western blot bands (G) and quantification of the antioxidant marker Nrf2 (H) and its binding partner Keap1 (I). (J–L) Expression and phosphorylation levels of relevant markers in the PI3K-AKT antiapoptosis pathway. Data were presented as mean ± SD (n = 3). *, $p < 0.05$, **, $p < 0.01$, compared with the IL-1β group; #, $p < 0.05$, ##, $p < 0.01$, ###, $p < 0.001$, compared with the control group. (M–Q) RT-qPCR analysis showing mRNA levels of Nrf2 (M), Nqo1 (N), Fas (O), Bax (P), and Bcl2 (Q) in different groups. Quantitative results were normalized to GAPDH and data were presented as mean ± SD (n = 3). *, $p < 0.05$, ***, $p < 0.001$ compared with the IL-1β group; #, $p < 0.05$, ##, $p < 0.01$, ###, $p < 0.001$, compared with the control group. (For interpretation of the references to color in this figure legend, the reader is referred to the Web version of this article.)

Col2 and Mmp13 were further confirmed through cellular immunofluorescence (Fig. 3E and F) and quantitative analysis of fluorescence intensity (Fig. 3G and H). To further confirm these changes at the gene expression level, RT-qPCR experiments were conducted to detect the expression levels of Col2, Sox9 and Mmp13. Results showed transcriptional changes consistent with that from WB experiments (Fig. 3I, J, K). Moreover, Acan, another crucial component of the ECM, was visualized by Alcian blue staining (Fig. 3L). As anticipated, IL-1β stimulation reduced the production of Acan. And LDH@TAGel exhibits the best efficacy for alleviating Acan degradation among the three materials, indicating its notable defensive function against ECM degradation. Collectively, our findings suggest that LDH@TAGel possesses a protective effect on IL-1β-induced chondrocyte degeneration.

3.5. RNA-seq analysis of IL-1β-induced chondrocytes treated with LDH@TAGel

Transcriptome RNA sequencing was conducted on chondrocytes to investigate the underlying mechanism of LDH@TAGel treatment. Total RNA for RNA-seq was extracted from chondrocytes exposed to IL-1β and LDH@TAGel (treatment group) and IL-1β alone (OA group). A total of 882 genes were analysed for significant changes in expression, with adjusted $p < 0.05$ and log2FC above or below the cut-off (>1, <-1). By comparing the treatment group to the OA group, we observed that 362 genes were upregulated and 520 genes were downregulated (Fig. S3). The results from principal component analysis (PCA) (Fig. S4) and sample-to-sample clustering analysis (Fig. S5) indicate a clear distinction between the two groups. Upon LDH@TAGel treatment, the ECM anabolic markers, such as Col2a1, Sox9 and Acan, exhibited upregulation, as observed in Fig. 4A and B. Conversely, the ECM catabolic markers, such as Mmp13 and Adamts5, displayed downregulation. Additionally, the downregulation of Nos2 was observed, which is a pivotal gene for the production of ROS and RNS. Kyoto Encyclopedia of Genes and Genomes (KEGG) enrichment analyses were performed to identify pathways that were significantly enriched following LDH@TAGel treatment (Fig. 4C). Among the top 20 enriched pathways, "ECM-receptor interaction" and "PI3K-Akt signalling pathway" were identified. To further evaluate biological processes from a system perspective, we performed gene set enrichment analysis (GSEA). The high negative values for the normalized enrichment score (NES) indicate that oxidative stress (Fig. 4D) and apoptotic processes (Fig. 4E) were inhibited in chondrocytes upon application of LDH@TAGel. Collectively, the results of transcriptome sequencing indicate that LDH@TAGel may protect the ECM through mechanisms involving the inhibition of oxidative stress and apoptosis.

3.6. In vitro antioxidant and antiapoptotic activity evaluation

The in vitro antioxidant activity of the materials was measured by a DPPH scavenging experiment. DPPH is a stable free radical compound that exhibits a purple colour and possesses a distinct UV–vis absorption peak at 517 nm. This compound can be efficiently reduced by antioxidant substances, making it a suitable indicator for evaluating the in vitro radical scavenging potential [48]. As shown in Fig. 5A, TAGel and LDH@TAGel effectively maintained the original DPPH elimination characteristics of TA, as evidenced by the change in solution colour from purple to yellow. LDH did not exhibit significant DPPH elimination, as shown by the unchanged solution colour. Quantitative analysis at 517 nm was further conducted, revealing the satisfactory antioxidant activity of TAGel and LDH@TAGel (Fig. 5B). The antioxidant activity of TAGel and LDH@TAGel shows a TA dose-dependent character, as shown in Fig. S6. However, LDH alone did not demonstrate significant DPPH scavenging activity across all concentrations (Fig. S6).

In vivo antioxidant activity was further evaluated within chondrocytes. During cellular oxidative stress, ROS and RNS are overproduced and reflect the level of oxidative stress. RNS production in culture medium exhibited a dramatic increase under IL-1β stimulation, as measured by the Griess assay (Fig. 5C). Both TAGel and LDH@TAGel could effectively decrease RNS levels in vivo. Interestingly, LDH alone also possessed anti-RNS activity (Fig. 5C). Based on the findings above (Fig. 5A and B), LDH does not exhibit direct free radical scavenging in vitro. Therefore, we hypothesize that the release of strontium could enhance the efficacy of antioxidant enzymes within cells, thereby regulating oxidative stress in vivo. The DCFH-DA probe can enter cells and release fluorescence in the presence of ROS. As shown in Fig. 5D, TAGel, LDH and LDH@TAGel all effectively reduced intracellular ROS levels, which is consistent with their ability to eliminate RNS.

Oxidative stress has been shown to facilitate cell apoptosis through protein/lipid peroxidation [47,49]. Thus, Annexin V-FITC/PI staining was employed to determine the apoptosis ratio of chondrocytes (Fig. 5E and F). Under IL-1β treatment, the apoptosis ratio of chondrocytes increased significantly from 9.34% ± 0.20% (CON) to 26.59% ± 1.85% (IL-1β). In contrast, the ratio of apoptotic cells was reduced to 22.84% ± 0.92% (TAGel), 19.36% ± 4.74% (LDH), and 15.76% ± 0.20% (LDH@TAGel) in the treatment groups. LDH@TAGel suppressed cell apoptosis most effectively. In summary, LDH@TAGel effectively integrates the individual functionalities of TA and LDH, thereby reducing the level of oxidative stress. This effect is achieved through both direct engagement with free radicals and the modulation of the inherent antioxidant capacity within chondrocytes.

Several pathway markers that possess antioxidant or antiapoptotic potential were further examined through western blot and RT-qPCR. Nrf2 plays a crucial role in mitigating oxidative damage, as it can upregulate the expression of antioxidant enzymes, while Keap1 acts as a binding partner for Nrf2 [50]. The stimulation of IL-1β resulted in a decrease in both Nrf2 and Keap1 expression (Fig. 5G–I). Conversely, chondrocytes treated with LDH@TAGel exhibited upregulation of these two markers. This upregulation effect was most significant in the LDH@TAGel group, followed by the LDH and TAGel groups. These findings indicate that IL-1β exerts a detrimental effect on antioxidant enzymes, whereas LDH@TAGel may effectively activate the antioxidant system. Pi3k/Akt signalling has been shown to possess anti-inflammatory and antiapoptotic properties in various cell types and tissues, while the inactivation of Akt leads to increased apoptosis and

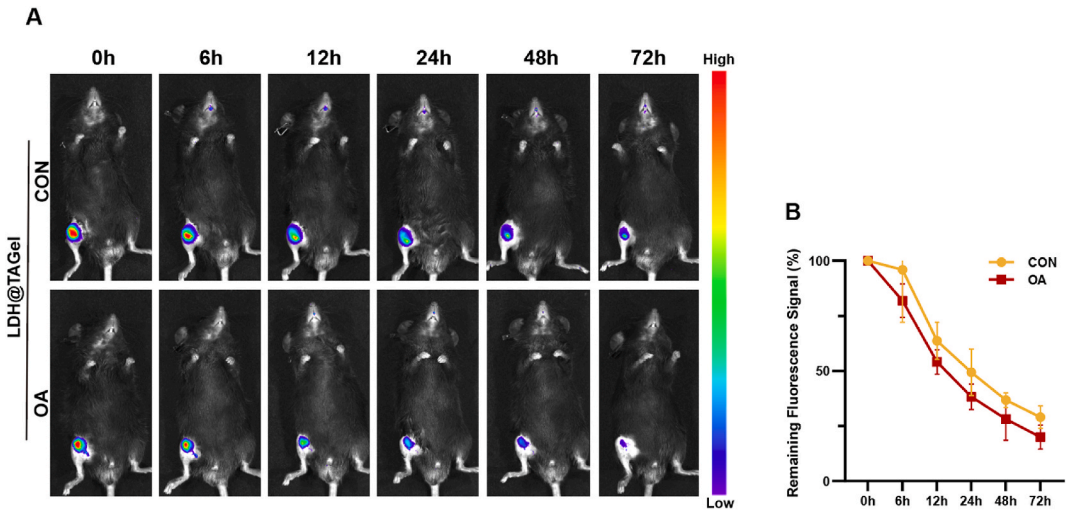

Fig. 6. In vivo retention and responsive release of LDH@TAGel. (A) Fluorescence images of Cy5-labelled LDH@TAGel in normal mice (upper panel) and OA mice with ACLT (lower panel) at different time points. (B) Remaining fluorescence signals normalized to that at 0 h. Data were presented as mean ± SD (n = 3).

inflammation [33,51]. Thus, we next examined the phosphorylation level of Pi3k and Akt in IL-1β- and material-treated chondrocytes. As depicted in Fig. 5J-L, the phosphorylation of Pi3k and Akt was suppressed upon IL-1β stimulation. However, the phosphorylation levels were activated to varying degrees after cocultivation with the materials, with the LDH@TAGel group exhibiting the most pronounced activation. Additionally, RT-qPCR was employed to detect changes in the expression of genes related to oxidative stress and apoptosis pathways. As shown in Fig. 5M and N, after material treatment, the expression of the antioxidant-related genes Nrf2 and Nqo1 was upregulated to various extents, confirming the antioxidant capability of LDH@TAGel. The expression of pro-apoptotic genes Bax and Fas was suppressed (Fig. 5O and P), while the expression of the anti-apoptotic gene Bcl2 was enhanced (Fig. 5Q), further demonstrating LDH@TAGel's antiapoptotic ability.

In short, LDH@TAGel exhibits notable antioxidant and antiapoptotic properties, potentially attributable to its direct elimination of free radicals, enhancement of the Nrf2/Keap1 antioxidant system, and activation of the Pi3k/Akt antiapoptotic signalling pathway.

3.7. Retention and responsive release of LDH@TAGel in vivo

The in vivo release of LDH from LDH@TAGel was monitored by an in vivo imaging system (IVIS). LDH was labelled with Cy5 before encapsulation with TAGel. Then, the LDH(Cy5)@TAGel was injected into the joint cavity of mice. The fluorescence signals generated by Cy5 serve as an indicator of nanogel retention and LDH release in vivo. The elimination rate of LDH in knees was observed to be rapid, indicating the need for a carrier to sustainably release it (Fig. S7). The incorporation of TAGel effectively slowed the eliminate rate of LDH (Fig. S7). Specifically, the fluorescence intensity in the LDH group decreased to 64.10% at 6h and decreased to 11.45% after 72 h. In contrast, the LDH@TAGel group maintained a fluorescence intensity of 95.95% at 6h and decreased to 29.06% after 72 h. Subsequently, to investigate the impact of the inflammatory milieu on LDH@TAGel, we injected LDH@TAGel into OA-afflicted knees (Fig. 6A). The fluorescence intensity decreased to 81.93% at 6h and decreased to 19.97% after 72 h in osteoarthritic joints, which was notably lower than that observed in normal joints (Fig. 6B). This decline in fluorescence intensity indicates accelerated degradation of the TAGel carrier within the osteoarthritic joints. This phenomenon can be attributed to the elevated levels of Mmps present within the inflammatory milieu. In response to Mmps stimulation, the gelatin in TAGel undergoes hydrolysis, thereby exhibiting responsive release behavior. Upon the hydrolysis of gelatin, the LDH@TAGel can release LDH and TA. This dual-release property renders LDH@TAGel highly promising for meeting therapeutic demands in osteoarthritic conditions.

3.8. Therapeutic effect on OA In vivo

Anterior cruciate ligament transection (ACLT) was conducted on mice to establish an animal model of OA, as previously described [52]. The TAGel, LDH, and LDH@TAGel were administered to the mice 2 weeks post-operation by intra-articular injection with a frequency of once every 4 days for a duration of 3 weeks (Fig. 7A). Concurrently, both the ACLT group and the sham group were treated with saline at identical time intervals. The mice were euthanized 5 weeks after ACLT surgery. In the context of Safranin O/Fast staining, the ACLT group exhibited evident osteoarthritic characteristics, such as surface erosion and cartilage degeneration, whereas the TAGel, LDH, and LDH@TAGel treatment groups displayed fewer changes (Fig. 7B). Notably, the LDH@TAGel treatment group demonstrated the least pathological alterations, approaching those observed in the sham group. These findings were supported by the results obtained from HE staining, which revealed increased infiltration of inflammatory cells and surface damage in the cartilage of the OA group. Conversely, treatment with LDH@TAGel resulted in reduced inflammatory infiltration and preservation of cartilage integrity. Further assessment of pathological changes in each group was conducted using the OA Research Society International (OARSI) scoring method [53]. OARSI scoring is a widely utilized quantitative system for evaluating the extent of cartilage degeneration. As shown in Fig. 7C, the average score of the LDH@TAGel treatment group was the lowest among all three treatment groups. Furthermore, immunohistochemistry staining for Col2 and Mmp13 was performed to assess the presence of ECM-associated proteins within the cartilage (Fig. 7B). In the ACLT group, IHC staining revealed a substantial reduction in Col2, with sparse positive staining indicative of decreased anabolic activity. There was also a significant loss of chondrocytes, and an increase in fibrous tissue, which are hallmarks of severe OA pathology. In contrast, treatment with TAGel, LDH, and particularly LDH@TAGel, resulted in a more robust Col2 staining, with a higher density of positively stained chondrocytes, suggesting a substantial protective effect on cartilage cells and maintenance of ECM. Furthermore, the intensity and distribution of Mmp13 staining were markedly elevated in the OA group, denoting extensive cartilage degradation. While in the treatment groups, especially those treated with LDH@TAGel, there was a noticeable reduction in Mmp13 positive staining, indicating a decrease in the catabolic breakdown of cartilage. TUNEL

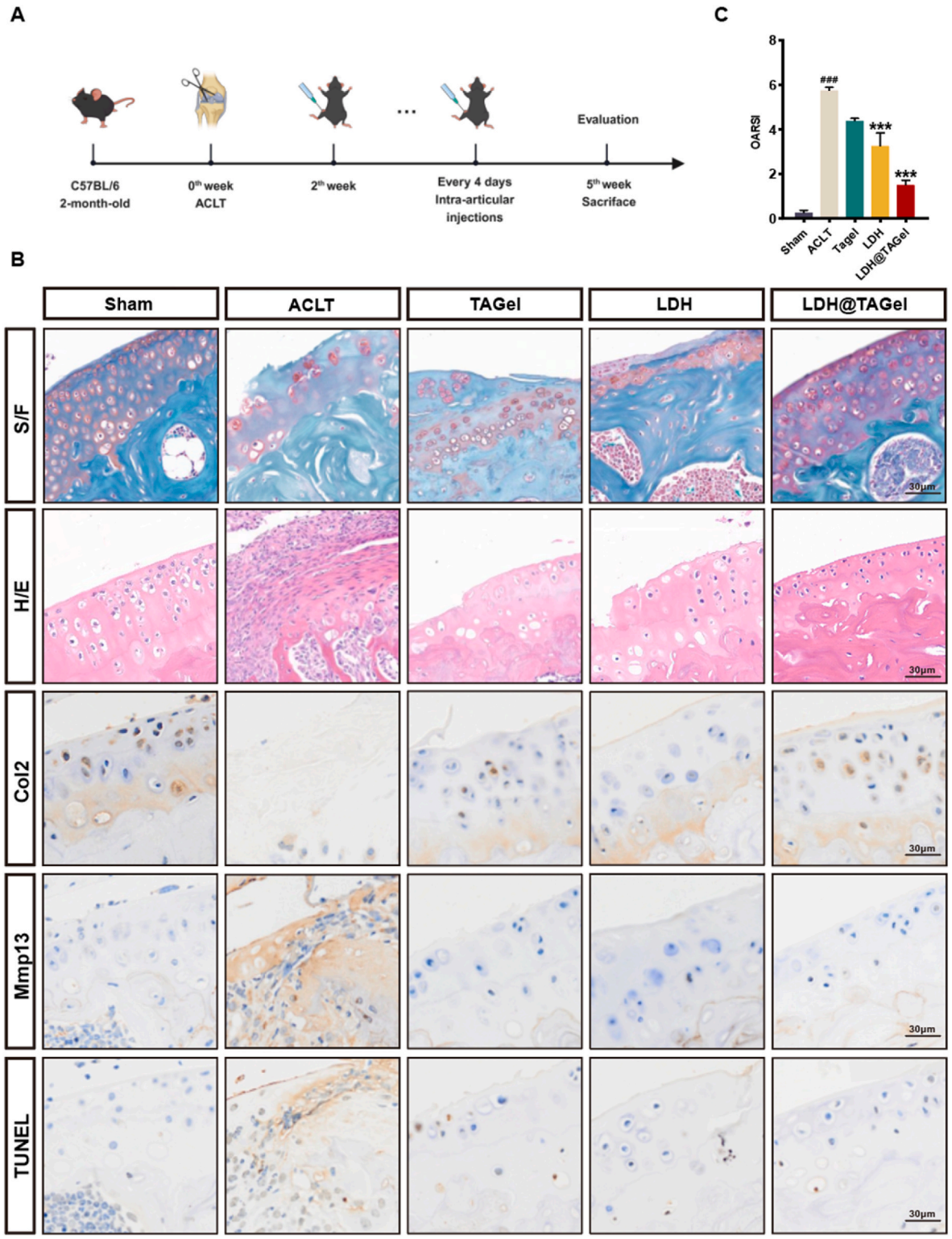

Fig. 7. In vivo attenuation of OA progression by LDH@TAGel. (A) Schematic description of ACLT animal experiments. (B) H/E and Safranin O-Fast Green staining to evaluate cartilage degeneration and therapeutic efficacy. IHC staining for visualization of Col2 and Mmp13 proteins and TUNEL staining showing apoptotic chondrocytes (C) Quantification analysis of the damage in each group with the OARSI scoring system. Data were presented as mean ± SD (n = 4). ***, $p < 0.001$, compared with the IL-1β group; ###, $p < 0.001$, compared with the control group. (For interpretation of the references to color in this figure legend, the reader is referred to the Web version of this article.)

staining is a method used to detect DNA fragmentation that results from apoptotic signaling cascades, serving as a marker for cell death. In the TUNEL results, the OA group demonstrated significant apoptotic activity, as evidenced by the high number of TUNEL-positive cells (Fig. 7B). This suggests heightened cell apoptosis within the cartilage, which is consistent with the degenerative processes associated with OA. On the contrary, the treatment groups, and particularly the LDH@TAGel group, showed fewer TUNEL-positive cells, suggesting that the treatments

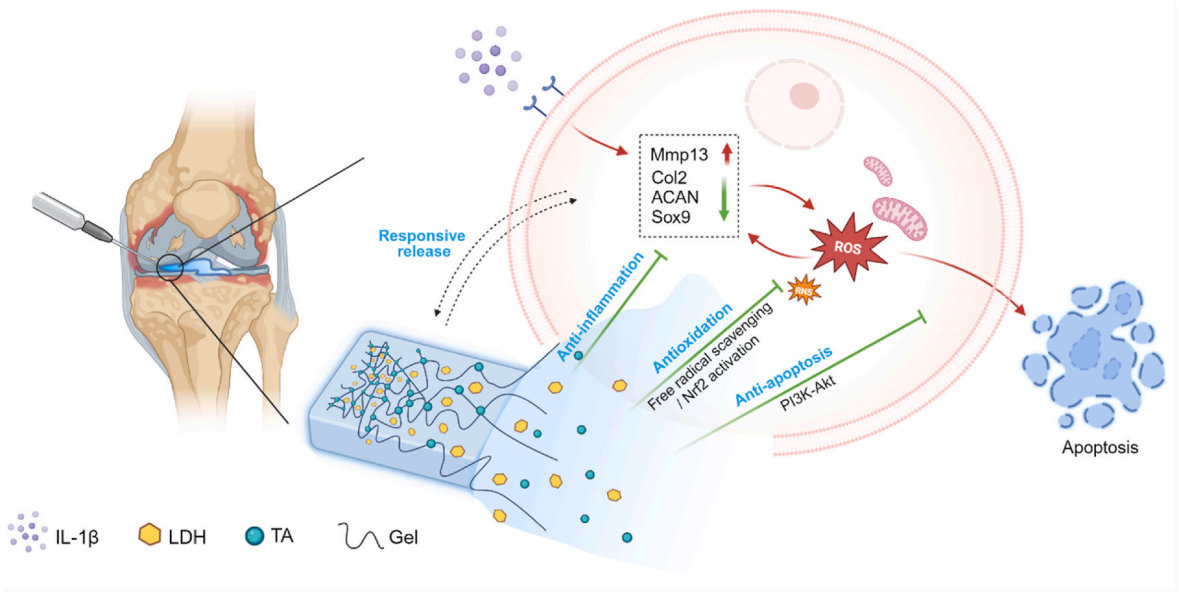

Scheme 1. Graphical abstract of the LDH@TAGel treatment mechanism for OA: Upon intra-articular injection, the LDH@TAGel degrade and release LDH and TA. The Sr^{2+}-containing LDH activates the antioxidative pathway (Nrf2). The TA directly scavenges free radicals. And then, the PI3K-Akt pathway was active, preventing chondrocytes from apoptosis. LDH@TAGel harnesses the anti-inflammatory properties of LDH and TA to promote ECM repair and reduce Mmp13 activity. Its inflammation-responsive release system administers treatment based on inflammation severity, preserving chondrocytes and ECM to mitigate OA progression.

provide a protective effect against apoptosis in chondrocytes in vivo. Overall, LDH@TAGel showed a promising therapeutic effect on a mouse ACLT osteoarthritis model.

4. Conclusion

In this study, we developed LDH@TAGel, a novel injectable and inflammation-responsive bioactive material for OA treatment. Its therapeutic effects are primarily achieved by protecting the ECM, suppressing oxidative stress, and preventing cell apoptosis, as summarized in Scheme 1. Within a certain concentration range, LDH@TAGel demonstrated good biocompatibility. Its ECM-protective capabilities are evidenced by the enhanced chondrocyte ECM secretion and simultaneous decreased secretion of destructive enzymes, thus reducing ECM degradation. The antioxidative effects of LDH@TAGel not only involve direct free radical scavenging but also improve the intrinsic antioxidative systems of chondrocytes. Furthermore, LDH@TAGel effectively suppressed inflammation-induced chondrocyte apoptosis and preserved the functional cell population. Additionally, LDH@TAGel ensures a controlled release of Sr^{2+} and TA in accordance with inflammation severity, thereby meeting therapeutic demands. This intelligent release ability and efficient cartilage-protection mechanism present a new strategy for OA treatment.

Funding

This research was partially supported by National Natural Science Foundation of China (82102600), National Natural Science Foundation of China (82272485), Shandong Provincial Natural Science Foundation (ZR202102210485) and Shandong Provincial Natural Science Foundation (ZR2021QB142).

Draft of Scheme 1 was created with BioRender.com.

CRediT authorship contribution statement

Changxing Liu: Writing – review & editing, Writing – original draft, Visualization, Validation, Methodology, Investigation, Conceptualization. **Yawei Sun:** Writing – review & editing, Writing – original draft, Visualization, Methodology, Investigation, Data curation, Conceptualization. **Dengju Li:** Validation, Methodology. **Fan Wang:** Methodology, Investigation. **Haojue Wang:** Validation, Investigation. **Senbo An:** Writing – review & editing, Validation, Supervision, Project administration, Funding acquisition, Conceptualization. **Shui Sun:** Writing – review & editing, Validation, Supervision, Project administration, Funding acquisition, Conceptualization.

Declaration of competing interest

The authors declare that they have no known competing financial interests or personal relationships that could have appeared to influence the work reported in this paper.

Data availability

Data will be made available on request.

Appendix A. Supplementary data

Supplementary data to this article can be found online at https://doi.org/10.1016/j.mtbio.2024.101034.

References

[1] S. Safiri, et al., Global, regional and national burden of osteoarthritis 1990-2017: a systematic analysis of the Global Burden of Disease Study 2017, Ann. Rheum. Dis. 79 (6) (2020) 819–828.
[2] K.D. Allen, L.M. Thoma, Y.M. Golightly, Epidemiology of osteoarthritis, Osteoarthritis Cartilage 30 (2) (2022) 184–195.
[3] S.L. Kolasinski, et al., 2019 American College of Rheumatology/Arthritis Foundation guideline for the management of osteoarthritis of the Hand, hip, and knee, Arthritis Care Res. 72 (2) (2020) 149–162.
[4] L. Yue, J. Berman, What is osteoarthritis? JAMA 327 (13) (2022) 1300.
[5] S. Muthu, et al., Failure of cartilage regeneration: emerging hypotheses and related therapeutic strategies, Nat. Rev. Rheumatol. 19 (7) (2023) 403–416.
[6] X. Zhou, et al., Moderate-intensity treadmill running relieves motion-induced post-traumatic osteoarthritis mice by up-regulating the expression of lncRNA H19, Biomed. Eng. Online 20 (1) (2021) 111.
[7] Y.-O. Son, et al., RNA-binding protein ZFP36L1 regulates osteoarthritis by modulating members of the heat shock protein 70 family, Nat. Commun. 10 (1) (2019) 77.
[8] G. Wood, et al., Osteoarthritis in people over 16: diagnosis and management-updated summary of NICE guidance, BMJ (Clinical Research ed.) 380 (2023) 24.

[9] Y. Lu, et al., Hierarchical functional nanoparticles boost osteoarthritis therapy by utilizing joint-resident mesenchymal stem cells, J. Nanobiotechnol. 20 (1) (2022) 89.
[10] N. de l'Escalopier, P. Anract, D. Biau, Surgical treatments for osteoarthritis, Annals of Physical and Rehabilitation Medicine 59 (3) (2016) 227–233.
[11] X. Du, et al., The role of TGF-beta3 in cartilage development and osteoarthritis, Bone Research 11 (1) (2023) 2.
[12] C. Deroyer, et al., CEMIP (KIAA1199) induces a fibrosis-like process in osteoarthritic chondrocytes, Cell Death Dis. 10 (2) (2019) 103.
[13] J.B. Catterall, et al., Aspartic acid racemization reveals a high turnover state in knee compared with hip osteoarthritic cartilage, Osteoarthritis Cartilage 24 (2) (2016) 374–381.
[14] H.J. Sim, et al., Augmented ERAD (ER-associated degradation) activity in chondrocytes is necessary for cartilage development and maintenance, Sci. Adv. 8 (3) (2022) eabl4222.
[15] C. Deng, et al., Bioactive scaffolds for regeneration of cartilage and Subchondral Bone interface, Theranostics 8 (7) (2018) 1940–1955.
[16] J.Y. Reginster, et al., Efficacy and safety of strontium ranelate in the treatment of knee osteoarthritis: results of a double-blind, randomised placebo-controlled trial, Ann. Rheum. Dis. 72 (2) (2013) 179–186.
[17] X. Shen, et al., High proportion strontium-doped micro-arc oxidation coatings enhance early osseointegration of titanium in osteoporosis by anti-oxidative stress pathway, Bioact. Mater. 10 (2022) 405–419.
[18] H.R. Kang, et al., Mg-Al and Zn-Al layered double hydroxides promote dynamic expression of marker genes in osteogenic differentiation by modulating mitogen-activated protein kinases, Adv. Healthcare Mater. 7 (4) (2018).
[19] S. Cheng, et al., Osteogenesis, angiogenesis and immune response of Mg-Al layered double hydroxide coating on pure Mg, Bioact. Mater. 6 (1) (2021).
[20] H. Fu, et al., Acid neutralization and immune regulation by calcium-aluminum-layered double hydroxide for osteoporosis reversion, J. Am. Chem. Soc. 144 (20) (2022) 8987–8999.
[21] R. Zhu, et al., Immunomodulatory layered double hydroxide nanoparticles enable neurogenesis by targeting transforming growth factor-β receptor 2, ACS Nano 15 (2) (2021) 2812–2830.
[22] X. Zhang, et al., ROS/RNS and base dual activatable merocyanine-based NIR-II fluorescent molecular probe for in vivo biosensing, Angew. Chem. 60 (50) (2021) 26337–26341.
[23] S. Zhang, et al., Nanomaterial-based reactive oxygen species scavengers for osteoarthritis therapy, Acta Biomater. 162 (2023) 1–19.
[24] M. Arra, et al., LDHA-mediated ROS generation in chondrocytes is a potential therapeutic target for osteoarthritis, Nat. Commun. 11 (1) (2020) 3427.
[25] H. Zhang, et al., Reactive oxygen species-responsive and scavenging polyurethane nanoparticles for treatment of osteoarthritis in vivo, Chem. Eng. J. (2021) 409.
[26] K. Sinha, et al., Oxidative stress: the mitochondria-dependent and mitochondria-independent pathways of apoptosis, Arch. Toxicol. 87 (7) (2013) 1157–1180.
[27] Y. Liu, et al., Arctiin-reinforced antioxidant microcarrier antagonizes osteoarthritis progression, J. Nanobiotechnol. 20 (1) (2022) 303.
[28] C.-C. Wang, et al., Hyaluronic acid injection reduces inflammatory and apoptotic markers through modulation of AKT by repressing the oxidative status of neutrophils from osteoarthritic synovial fluid, Int. J. Biol. Macromol. 165 (Pt B) (2020) 2765–2772.
[29] C. Pucci, et al., Tannic acid-iron complex-based nanoparticles as a novel tool against oxidative stress, ACS Appl. Mater. Interfaces 14 (14) (2022) 15927–15941.
[30] M.V. Lomova, et al., Multilayer capsules of bovine serum albumin and tannic acid for controlled release by enzymatic degradation, ACS Appl. Mater. Interfaces 7 (22) (2015) 11732–11740.
[31] J. Gao, et al., Overcoming barriers for intra-articular delivery of disease-modifying osteoarthritis drugs, Trends Pharmacol. Sci. 43 (3) (2022) 171–187.
[32] T.N. Doan, et al., Endothelin-1 inhibits size dependent lymphatic clearance of PEG-based conjugates after intra-articular injection into the rat knee, Acta Biomater. 93 (2019) 270–281.
[33] G. Li, et al., An injectable liposome-anchored teriparatide incorporated gallic acid-grafted gelatin hydrogel for osteoarthritis treatment, Nat. Commun. 14 (1) (2023) 3159.
[34] K.Y. Lu, et al., A novel injectable in situ forming gel based on carboxymethyl hexanoyl chitosan/hyaluronic acid polymer blending for sustained release of berberine, Carbohydr. Polym. 206 (2019) 664–673.
[35] W. Zhao, et al., Bioinspired nanospheres as anti-inflammation and antisenescence interfacial biolubricant for treating temporomandibular joint osteoarthritis, ACS Appl. Mater. Interfaces 14 (31) (2022) 35409–35422.
[36] S. Xue, et al., Cartilage-targeting peptide-modified dual-drug delivery nanoplatform with NIR laser response for osteoarthritis therapy, Bioact. Mater. 6 (8) (2021) 2372–2389.
[37] C. Deng, et al., Sophisticated magneto-mechanical actuation promotes in situ stem cell assembly and chondrogenesis for treating osteoarthritis, ACS Nano 17 (21) (2023) 21690–21707.
[38] S.W. Yang, et al., High-density horizontal stacking of chondrocytes via the synergy of biocompatible magnetic gelatin nanocarriers and internal magnetic navigation for enhancing cartilage repair, Polymers 14 (4) (2022).
[39] J. Liu, et al., Encapsulation of Curcumin nanoparticles with MMP9-responsive and Thermos-sensitive hydrogel improves Diabetic Wound healing, ACS Appl. Mater. Interfaces 10 (19) (2018) 16315–16326.
[40] Y. Sun, et al., Hierarchical cross-linked poly(caprolactone-co-urethane) toward connective tissue-like properties and multifunctional integration, Chem. Mater. 31 (22) (2019) 9295–9306.
[41] F. Rainer, V. Ribitsch, [Viscoelastic properties of normal human synovia and their relation to biomechanics], Zeitschrift Fur Rheumatologie 44 (3) (1985) 114–119.
[42] Z. Gong, et al., CircZSWIM6 mediates dysregulation of ECM and energy homeostasis in ageing chondrocytes through RPS14 post-translational modification, Clin. Transl. Med. 13 (1) (2023) e1158.
[43] C.R. Liao, et al., Advanced oxidation protein products increase TNF-α and IL-1β expression in chondrocytes via NADPH oxidase 4 and accelerate cartilage degeneration in osteoarthritis progression, Redox Biol. 28 (2020) 101306.
[44] S. Kim, et al., Tankyrase inhibition preserves osteoarthritic cartilage by coordinating cartilage matrix anabolism via effects on SOX9 PARylation, Nat. Commun. 10 (1) (2019) 4898.
[45] H. Song, K.H. Park, Regulation and function of SOX9 during cartilage development and regeneration, Semin. Cancer Biol. 67 (Pt 1) (2020) 12–23.
[46] Y. Wu, et al., Metabolite asymmetric dimethylarginine (ADMA) functions as a destabilization enhancer of SOX9 mediated by DDAH1 in osteoarthritis, Sci. Adv. 9 (6) (2023) eade5584.
[47] Z. Jiang, et al., Cartilage targeting therapy with reactive oxygen species-responsive nanocarrier for osteoarthritis, J. Nanobiotechnol. 20 (1) (2022) 419.
[48] M.B. Adekola, et al., In-vitro antioxidant and anti-inflammatory activities of ethanol stem-bark extract of Blighia sapida K.D. Koenig, J Pharm Anal 12 (2) (2022) 350–354.
[49] M. Ramosaj, et al., Lipid droplet availability affects neural stem/progenitor cell metabolism and proliferation, Nat. Commun. 12 (1) (2021) 7362.
[50] R. Liang, et al., Implantable and degradable antioxidant poly(ε-caprolactone)-lignin nanofiber membrane for effective osteoarthritis treatment, Biomaterials 230 (2020) 119601.
[51] Z. Xia, et al., GNA13 regulates BCL2 expression and the sensitivity of GCB-DLBCL cells to BCL2 inhibitors in a palmitoylation-dependent manner, Cell Death Dis. 12 (1) (2021) 54.
[52] J. Lorenz, S. Grässel, Experimental osteoarthritis models in mice, Methods Mol. Biol. 1194 (2014) 401–419.
[53] S.S. Glasson, et al., The OARSI histopathology initiative - recommendations for histological assessments of osteoarthritis in the mouse, Osteoarthritis Cartilage 18 (Suppl 3) (2010) S17–S23.